In Vivo Co-distribution of Fibronectin and Actin Fibers in Granulation Tissue: Immunofluorescence and Electron Microscope Studies of the Fibronexus at the Myofibroblast Surface

IRWIN I. SINGER, DOUGLAS W. KAWKA, DIANA M. KAZAZIS, and RICHARD A. F. CLARK*

*Department of Experimental Pathology, Merck Sharp & Dohme Research Laboratories, Rahway, New Jersey 07065; and *Department of Medicine, National Jewish Hospital and Research Center, Denver, Colorado 80206*

ABSTRACT The fibronexus (FNX), a very close transmembrane association of individual extracellular fibronectin fibers and actin microfilaments, was found previously at the substrate-binding surface of fibroblasts in tissue culture (Singer, I. I., 1979, *Cell*, 16:675–685). To determine whether the fibronexus might be involved in fibroblast adhesion during wound healing in vivo, we looked for co-localization of actin and fibronectin in granulation tissue formed within full-thickness guinea pig skin wounds. At 7–9 d, most of the actin fibers were observed to be coincident with congruent fibronectin fibers using double-label immunofluorescence microscopy. These fibronectin and actin fibers were co-localized at the myofibroblast surface surrounding the nucleus, and along attenuated myofibroblast processes which extended deeply into the extracellular matrix. This conspicuous co-distribution of fibronectin and actin fibers prompted us to look for fibronexuses at the myofibroblast surface with electron microscopy. We observed three kinds of FNXs: (*a*) tandem associations between the termini of individual extracellular fibronectin fibers and actin microfilament bundles at the tips of elongate myofibroblast processes, (*b*) plaque-like and, (*c*) track-like FNXs, in which parallel fibronectin and actin fibers were connected by perpendicular transmembranous fibrils. Goniometric studies on the external and internal components of these cross-linking fibrils showed that their membrane-associated ends are probably co-axial. Using immunoelectron microscopy on ultrathin cryosections, we confirmed that the densely staining external portion of these various FNXs does indeed contain fibronectin. The finding that these FNXs appear to connect collagen fibers to intracellular bundles of actin microfilaments is particularly significant. Our studies strongly suggest that the fibronexus is an important in vivo cell surface adhesion site functioning in wound repair, and perhaps within fibronectin-rich tissues during embryogenesis, tumor growth, and inflammation.

The in vitro enhancement of fibroblast adhesion and spreading by fibronectin has been well documented (20, 29, 55, 56), whereas the importance of the cytoskeleton in these processes has only recently been realized (23, 26, 27, 42, 43, 46). The observation that actin microfilament bundles (stress fibers) are highly developed in well-spread stationary fibroblasts in vitro (23, 27, 35, 43, 46), and are diminished in mobile and transformed cells, strongly suggests a dominant role for the cytoskeleton in the fibroblast-to-substrate adhesion mechanism. A fascinating aspect of this phenomenon is the coincident distribution of fibronectin-containing extracellular matrix fibers and bundles of actin microfilaments on a global scale at the substrate adhesive surface (22, 26, 27). Electron microscopic studies of this substrate-binding plasma mem-

THE JOURNAL OF CELL BIOLOGY · VOLUME 98 JUNE 1984 2091–2106

brane have demonstrated that the fibronectin and actin fibers form transmembrane complexes composed of individual 5-nm microfilaments and fibronectin fibrils organized into a close one-on-one association called the fibronexus (42). Subsequent experiments have shown that vinculin, a component of focal contacts (5, 15), is also a constituent of those fibronexuses localized at the zones of close substrate apposition in stationary fibroblasts (27, 43, 46). These observations lead us to propose that the extracellular matrix and actin-cytoskeleton comprise a complex supramolecular assemblage which governs the process of fibroblast adhesion in vitro.

The purpose of our present work is to determine if the fibronexus is a dominant adhesive complex in vivo. Early granulation tissue of healing skin wounds was selected for this work because its myofibroblasts are rich in actin microfilaments (11), and are situated close to fibronectin-containing extracellular matrix fibers (7, 19, 38). In this paper, we show that an extraordinary degree of actin and fibronectin superimposition exists in granulation tissue, suggesting that the fibronexus is a prevalent structure at the myofibroblast plasma membrane. Furthermore, using ultrastructural, goniometric, and immunoelectron microscopic methods, we have observed that three different types of fibronexuses apparently attach myofibroblasts to their extracellular matrix. A preliminary report of our results was presented recently (45).

MATERIALS AND METHODS

Granulation Tissue: At 7 and 9 d before killing, full-thickness skin wounds were made with a 4-mm-diam biopsy punch along the depilitated flanks of 300–350 g female Hartley guinea pigs. Longitudinal strips of skin containing both 7- and 9-d wounds were dissected out and immediately immersed in fixative. The wounds were then rapidly excised from the surrounding skin and cut into quarters with razor blades. In this way, portions of the granulation tissue, which comprises a spherical plug located in the center of the wound, were rapidly exposed to the fixative. In addition, samples of subdermal striated muscle (panniculus carnosus) from the surrounding skin were also obtained to monitor the staining patterns of the antiactin antibodies.

Fixation: For immunofluorescence and immunoelectron microscopy, tissues were fixed in 3.5% formaldehyde (generated freshly from paraformaldehyde) and 1% glutaraldehyde in 0.1 M cacodylate buffer (pH 7.0) containing 0.1 M sucrose plus 4.5 mM $CaCl_2$. After 2 h and three changes of fixative at 23°C, the tissues were washed with 0.1 M cacodylate buffer containing 5 mM $CaCl_2$ and 5 mM $MgCl_2$ and stored in the latter buffer containing 0.1% NaN_3 at 4°C. Tissues intended for structural (nonimmunological) electron microscopic analysis were also preserved with a modification of the above fixative containing 2% glutaraldehyde and 1% tannic acid (pH 7.0).

Antibodies and Immunological Reagents: Antisera to human plasma fibronectin were raised in rabbits, and the IgG fraction was purified by chromatography on DEAE cellulose and precipitation with $(NH_4)_2SO_4$ as previously described (7, 8). Rabbit antifibronectin IgG was also affinity purified on a fibronectin immunoabsorbant (1.5 mg of purified human plasma fibronectin [46] per 3 ml of washed glutaraldehyde-activated Ultrogel ACA-22 beads (LKB Instruments, Inc., Gaithersburg, MD) (47)). The fibronectin antibodies were tested by immunoelectrophoresis and immunofluorescence microscopy of human and hamster fibroblast (WI-38, Nil8) monolayers and found to be monospecific for fibronectin (46). Ascites fluid containing monoclonal anti-chicken gizzard actin IgM was a generous gift from Dr. James Jung-Ching Lin of the Cold Spring Harbor Laboratories (Cold Spring Harbor, NY). This antibody has been shown to react immunospecifically with actin from chicken gizzards, mouse 3T3 cells, rat fibroblasts, and gerbil fibroma cells. Biotinylated affinity-purified goat anti-rabbit IgG (H&L, heavy and light chains), affinity-purified biotinylated horse anti-mouse IgG (H&L) which recognizes mouse IgM, avidin-D, fluorescein avidin-D, rhodamine avidin-D, ferritin avidin-D, and biotinylated ferritin were purchased from Vector Laboratories, Inc. (Burlingame, CA). The secondary rabbit and mouse antibodies have not been found to cross-react in immunodiffusion tests.

Production of 1-μm Frozen Sections for Immunofluorescence Microscopy: Approximately 1-mm^3 blocks of guinea pig granulation tissue or subdermal striated muscle fixed as detailed above were infiltrated overnight with 2.3 M sucrose in 0.1 M phosphate buffer (pH 7.2) containing 0.1% NaN_3. Samples were then mounted on silver Reichert mounting stubs with OCT compound (Lab-Tek Div., Miles Laboratories Inc., Naperville, IL), and frozen rapidly in refreezing liquid N_2-cooled Freon 22 (99.9% pure, Matheson Div., Searle Medical Products, East Rutherford, NJ). 1-μm frozen sections were cut with dry glass knives on a Reichert FC-2 low temperature ultramicrotome at a specimen temperature of −55°C and a knife temperature of −50°C. The sections were picked up using the sucrose droplet method of Dr. K. T. Tokuyasu (49), placed on polylysine-treated glass slides and stored under sucrose solution at 4°C.

Double Immunofluorescence Staining for Fibronectin and Actin: After extensive washing in 0.1 M Tris HCl buffer (pH 7.5) at 37°C and treatment with lysine (5 mg/ml in 0.1 M phosphate buffer pH 7.8) to remove the sucrose overlay and quench any endogenous aldehydes, the tissue sections were treated via the following series of reagents in moist chambers at 23°C, with seven washes of 0.1 M phosphate buffer (pH 7.8) between each step: (*1*) affinity-purified rabbit antifibronectin IgG (27 μg/ml in 0.1 M phosphate, pH 7.2), or rabbit antifibronectin IgG (100 μg/ml in pH 7.8 0.1 M phosphate), 45 min; (*2*) affinity-purified biotinylated goat anti-rabbit IgG (H&L) (10–50 μg/ml in 0.1 M phosphate buffer, pH 7.8), 45 min; (*3*) rhodamine avidin-D (20–50 μg/ml in 0.1 M $NaHCO_3$, pH 8.0), 30 min; (*4*) biotin for 15 min (25 μg/ml in 0.1 M $NaHCO_3$, pH 8.0) to prevent the avidin introduced in step *3* from binding the next biotinyl-antibody; (*5*) monoclonal mouse antiactin IgM (50 μg/ml in 0.1 M phosphate buffer, pH 7.8), 45 min; (*6*) biotinylated affinity-purified horse anti-mouse IgG (H&L) (10–50 μg/ml in 0.1 M phosphate buffer, pH 7.8), 45 min; (*7*) fluorescein avidin-D (20–50 μg/ml in 0.1 M $NaHCO_3$, pH 8.0), 30 min; (*8*) coverslips were mounted with 4% *n*-propyl gallate in 0.1 M $NaHCO_3$ (pH 8.0) and 80% glycerol. The *n*-propyl gallate was used as an antioxidant to reduce photobleaching of these fluorochromes (16). To test the immunospecificity of this double-labeling protocol, and to assess the possible levels of background staining, we incubated the primary antibody solutions (steps *1* and *5* above) with excess antigen: 200 μg of chick embryo fibroblast fibronectin (46) per 100 μg antifibronectin IgG, and 100 μg of chicken gizzard actin (Sigma Chemical Co., St. Louis, MO) per 50 μg of mouse antiactin IgM. The reaction was run in 0.1 M phosphate buffer (pH 7.8) for 16 h at 23°C with constant agitation followed by centrifugation for 15 min at 15,000 *g*. Alternatively, IgG and IgM from unimmunized animals, or 0.1 M phosphate buffer, were employed in place of either or both primary antibodies in steps *1* and *5* above.

Immunoelectron Microscopic Labeling Techniques: The avidin-biotin labeling method used as above for immunofluorescence microscopy was modified for the postsectioning staining of fibronectin in ultrathin cryosections of guinea pig granulation tissue. All immunological and marker solutions contained 0.1% BSA (Sigma Chemical Co.; crystalized, lyophilized, and globulin free) and 0.1% NaN_3. The following labeling steps were performed directly on the grids with intervening 0.1 M Tris buffer washes at 23°C: (*1*) affinity-purified rabbit antifibronectin IgG (as step *1* above), (*2*) affinity-purified biotinyl-goat anti-rabbit IgG (as step *2* above), and (*3*) 50–100 μg/ml ferritin-conjugated avidin in 0.1 M $NaHCO_3$, pH 8.2, for 20 min. As an alternate labeling method, the grids were treated with 50 μg/ml of unlabeled avidin-D after step *2* for 20 min, followed by 100 μg/ml biotinylated ferritin in 0.1 M $NaHCO_3$, pH 8.3, for 20 min. We found that the biotinyl ferritin produced more intense labeling of fibronectin than the avidin-ferritin.

Immunofluorescence Microscopy: Double-stained 1-μm frozen sections were studied with a Zeiss universal photomicroscope ultraphot equipped with a 100 W high pressure mercury vapor lamp and an epifluorescence condenser III RS. For fluorescein-specific fluorescence, a selective exciter filter (BP 485/20 nm) was used in combination with a narrow band barrier filter (520–560 nm) in order to prevent rhodamine "bleed through" in double-stained specimens. Selective rhodamine fluorescence was obtained using a BP 546/12 nm exciter filter and an LP 590-nm barrier filter. The tissues were photographed with either a 63× or 100× Zeiss planapochromatic objective lens (numerical apertures of 1.4 or 1.3, respectively) equipped with phase rings. Black and white photomicrographs were produced on Ilford HP5 35-mm fine grain film processed at either 1600 ASA with Acufine, or at 3200 ASA with Ilford Microphen fine grain developers. Kodak Ektachrome film was used at 800 ASA for color micrography.

Structural (Nonimmunological) Electron Microscopy: After the fixed granulation tissue blocks were thoroughly washed in 0.1 M Na cacodylate containing 5 mM $CaCl_2$ plus 5 mM $MgCl_2$, they were treated with 2% OsO_4, dehydrated with ethanols, and infiltrated in epon. Semithin (1 μm) plastic sections were prepared for each block to verify that it consisted of granulation tissue rather than the surrounding dermis. Silver-gray ultrathin sections were stained with saturated alcoholic uranyl acetate plus Reynold's lead citrate (39) and studied at 80–100 kV under a JEOL 200 CX transmission electron microscope equipped with a eucentric side entry goniometer and wide

angle objective lens pole piece (HA-PP) capable of ±60° specimen tilt, 360° rotation, and 4.5 Å point-to-point resolution (BSR specimen holder). A column vacuum of 10^{-7} mm Hg was obtained with a liquid N_2 baffle on the lower diffusion pump, and a liquid N_2-ACS anticontamination device surrounding the specimen; the beam current was 6–7 μA. In this way, multiple exposures of the same specimen could be made for our goniometric studies without observable contamination or damage to our samples. Objective lens apertures of 40–60 μm were used, and the objective lens astigmatism was corrected directly on the specimen being studied after each tilt of the specimen holder.

Ultrathin Cryosectioning for Immunoelectron Microscopy: Specimens of fixed granulation tissue were infiltrated with 2.3 M sucrose in 0.1 M phosphate buffer (pH 7.2) containing 0.1% NaN_3, and rapidly frozen onto silver Reichert specimen stubs in liquid N_2-cooled Freon 22 as above. Semithin sections were made first to study the tissue with phase-contrast microscopy. Dry ultrathin frozen sections with a gold-pink interference color (~80 nm) were then cut with free broken glass knives on a Reichert Ultracut ultramicrotome, utilizing the Reichert FC-4 cryosectioning attachment at a knife temperature of −90°C and a specimen temperature of −95°C. Ribbons of ultrathin cryosections were picked up and processed on Formvar-carbon–coated nickel grids according to the sucrose droplet and the positive adsorption staining methods of Dr. K. T. Tokuyasu (48, 49). These techniques were modified in the following manner: (*a*) Agarose plates and sucrose pick-up solutions were made without gelatin as this significantly reduced the background staining. (*b*) The grids were treated with 0.1 M Tris buffer, pH 7.8, to quench endogenous aldehyde groups before staining with the primary antibody; this buffer was also used for washing between the various immunological labeling steps (see above). (*c*) Bismuth subnitrate was used as detailed by Ainsworth and Karnovsky (1) to enhance the contrast of the ferritin label before staining with neutral uranyl acetate (pH 7.0). (*d*) The final embedment consisted of 0.8% polyethylene glycol (1,540 mol wt, Union Carbide Corp., Somerset, NJ), 0.2% methyl cellulose (1,500 cps, Dow Chemical Co., Indianapolis, IN), and 0.02% acidic uranyl acetate.

RESULTS

Immunospecificity of Fibronectin and Actin Staining Patterns

We used the avidin-biotin immunostaining technique to localize fibronectin and actin simultaneously in granulation tissue sections rather than more conventional indirect double-labeling methods. This method was chosen because we often encountered heavy nonspecific labeling in attempting to immunostain sections of skin with fluorochrome-conjugated secondary antibodies. In addition, the biotin-avidin system offers greater sensitivity and increased stability because of the high binding affinity between avidin and biotin (10^{15} M^{-1}) (54).

To verify that the fluorescent staining patterns observed with this double label avidin-biotin method were immunospecific, and were not caused by endogenous avidin binding activity (54), we conducted a number of control experiments (Fig. 1). If nonimmune IgG of the appropriate species was substituted for the primary antibody in either the first (fibronectin) or second (actin) tier of stains, then the staining pattern corresponding to that antibody was selectively abolished with no effect on the labeling pattern generated by the complementary series of labels (Fig. 1, *A–C* and *D–F*). Similar results were obtained by omitting antibodies from the primary step in either the first or second staining tier. Preincubation of the fibronectin and/or actin antibodies with an excess of the corresponding antigen also selectively inhibited each immunolabeling pattern (Fig. 1, *G–I*). These experiments indicate that the fibrillar staining we observed in guinea pig granulation tissue represents the fibronectin and actin distribution of that tissue. Our controls also illustrate the effectiveness of the biotin blocking step between the antiactin and antifibronectin staining tiers, and in addition show that the biotinylated secondary antibodies that we used do not cross-react (Fig. 1, *A–F*). As an additional check of the staining specificity of the monoclonal actin antibody, we also labeled the subdermal striated muscle of the panniculus carnosus. A brilliant striated pattern of immunofluorescence staining was localized at the I bands of the muscle (Fig. 1 *J*), which could be blocked by pretreatment of the actin antibody with purified chicken gizzard actin (Fig. 1 *K*). On the basis of these results, we are confident in the immunospecificity of the actin and fibronectin patterns reported below.

Co-distribution of Actin and Fibronectin Fibers along the External Surfaces and Cellular Processes of Myofibroblasts

Double-label immunofluorescence microscopy using the biotin-avidin method on 1-μm frozen sections of granulation tissue of 7–9-d-old guinea pig skin wound revealed that actin and fibronectin were distributed as many fine delicate fibers (Figs. 2–4). These actin and fibronectin fibers were usually congruent and their distributions appeared to be highly coincident (Figs. 2 and 3). However, a few examples of fibronectin fibers that were not labeled with actin antibody (Fig. 2, *A* and *B*) and actin fibers that lacked fibronectin staining (Fig. 2, *C* and *D*) were observed. We also found several examples of actin fibers that were only partially stained for fibronectin over a fraction of their length (Fig. 2, *C* and *D*). Perhaps this pattern represents an actin-filled cellular process surrounded by fibronectin at its tip, or maybe the sectioning process has inadvertently cut one or the other fibers out of the tissue. (These noncongruent but closely opposed actin and fibronectin fibers constitute additional evidence for the independence of each staining tier, thus further attesting to the immunospecificity of our double labeling method). In spite of these local differences, the distribution of fibronectin and actin fibers appeared to be highly coincident throughout most of the granulation tissue as assayed using color photomicrographs (Fig. 3). When the actin pattern (viewed using fluorescein avidin as in Fig. 3 *A*) and the corresponding fibronectin distribution (visualized with rhodamine avidin and shown in Fig. 3 *B*) of a double-stained section were combined via double exposure (Fig. 3 *C*), both actin and fibronectin fibers appeared to co-distribute perfectly. The ability of the double color exposure method to detect noncoincident red and green fibers was tested by intentionally misaligning both patterns; in this instance the fibronectin and actin components of each fiber could be seen individually (Fig. 3 *D*, double arrowhead).

We also attempted to localize the acto-fibronectin fibers with respect to granulation tissue myofibroblasts using phase-contrast microscopy in conjunction with double-label immunofluorescence microscopy (Fig. 4). As illustrated in Fig. 4 *C* (arrowheads), the intercellular portion of the granulation tissue contains many dense elongated structures which are probably the extended processes of the constituent myofibroblasts. These attenuated cellular extensions are closely associated with double-stained acto-fibronectin fibers (see corresponding arrowheads in Fig. 4, *A* and *B*). The fibrous complexes of actin and fibronectin are also closely apposed to the perimeter of the myofibroblast in the area surrounding the nucleus (Fig. 4, *D–F*). In this example, the actin fibers are localized close to the surface of the myofibroblast (Fig. 4 *E*) and are absent from the more internal portions of the cytoplasm.

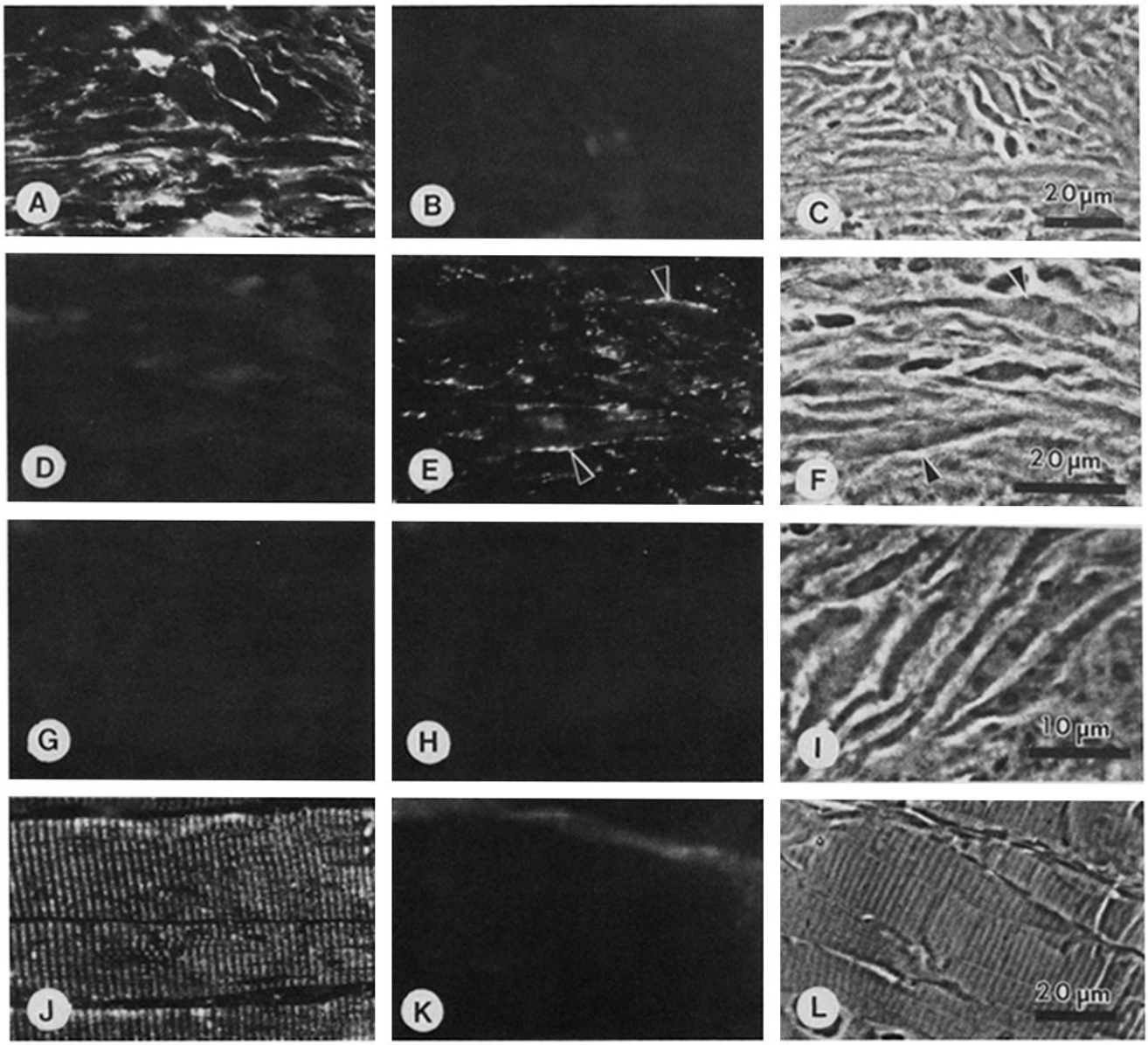

FIGURE 1 Immunospecificity of the fibronectin and actin staining patterns on 1-μm cryosections of 9-d guinea pig granulation tissue labeled with the two chromophore avidin-biotin procedure described in Materials and Methods. The fibronectin was stained with rhodamine avidin while the actin was labeled with fluorescein avidin so that both staining patterns (or appropriate controls) could be visualized in the same area using specific combinations of interference filters. *A–C* show a section stained with affinity-purified rabbit antifibronectin IgG (27 μg/ml) and IgM from nonimmunized mice (50 μg/ml). (*A*) Rhodamine optics reveals a delicate fibrous fibronectin staining pattern; (*B*) same region viewed with fluorescein filters exhibits very little background staining from nonimmune mouse antibodies; (*C*) phase-contrast micrograph of *A* and *B*. *D–F* exhibit granulation tissue incubated with monoclonal antiactin mouse IgM (50 μg/ml) and 100 μg/ml IgG from an unimmunized rabbit. (*D*) No fibronectin fibers are displayed with the rhodamine filters whereas (*E*) actin fibers located at the periphery of the myofibroblasts (arrowheads) are seen in the same area with fluorescein optics. (*F*) Phase-contrast micrograph of *D* and *E*; arrowheads depict myofibroblasts shown in *E*. *G–I* demonstrate that no staining is obtained if the actin and fibronectin antibodies are pretreated with excess corresponding antigen as described in Materials and Methods. (*G*) Rhodamine avidin shows no rabbit antifibronectin staining; (*H*) corresponding area exhibits no actin staining with fluorescein avidin; (*I*) myofibroblasts of regions *G* and *H* seen under phase optics. Series *J–L* illustrates actin staining in cryosections of subdermal striated muscle. (*J*) The monoclonal actin antibody used in *E* above generates a striated staining pattern, which is blocked by pretreatment with excess actin (*K*). *L* exhibits the striations of the control section shown in *K*. (*A–C* and *J–L*) × 600; (*D–F*) × 860; (*G–I*) × 1,500.

Electron Microscopy of the Granulation Tissue

DENSELY STAINING FIBRONECTIN MATRIX AT THE MYOFIBROBLAST SURFACE: Specimens of granulation tissue from 7–9-d skin wounds were also prepared for fine structural analysis using the same animals upon which we conducted the double-label immunofluorescence studies. The myofibroblasts of this tissue were often organized into cords within the extracellular matrix. Their attenuated processes within these cords had significant amounts of densely stained fibrous material localized at their outer surfaces (Fig. 5*A*). Our immunoelectron microscopic experiments show that this

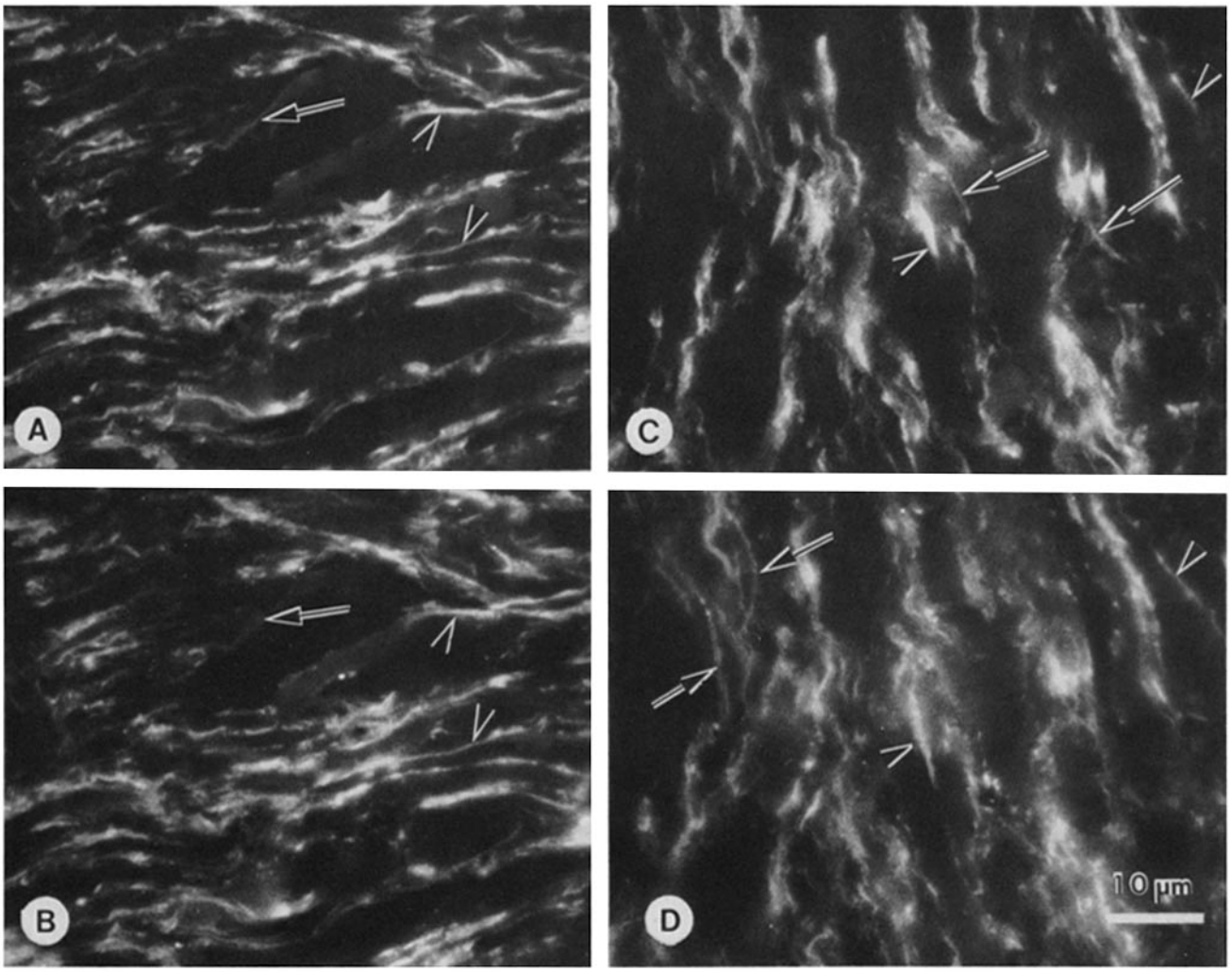

FIGURE 2 Co-distribution of fibronectin and actin fibers in double-stained 1-μm cryosections of guinea pig granulation tissue. *A* and *B* illustrate the extraordinary coincidence of congruent fibronectin and actin fibers (matching arrowheads). *A* is the fibronectin distribution visualized with rhodamine avidin (arrow indicates a fibronectin fiber which is actin negative), and *B* shows the actin pattern of the same site observed with fluorescein avidin (arrow depicts position of actin-lacking fibronectin fiber). The corresponding fibronectin (*C*) and actin (*D*) patterns of other granulation tissue regions are also highly coincident but not always co-extensive; matching arrowheads depict actin fibers that have fibronectin staining at only one end, while arrows indicate some fibronectin fibers (*C*) and actin bundles (*D*) that do not exhibit both proteins. × 1,350.

dense fibrillar cell surface matrix is rich in fibronectin antigens (see Fig. 10). Therefore, we shall refer to the dense membrane-associated extracellular matrix fibers described in the following ultrastructural experiments as fibronectin fibers.

CORTICAL ACTIN MICROFILAMENTS IN MYOFIBROBLASTS: Granulation tissue myofibroblasts contained many dense bundles of 5-nm actin-microfilaments (Fig. 5 *B*) localized at the cell surface. These microfilament bundles also filled the attenuated cellular processes located in the extracellular matrix (Fig. 5 *E*). Bundles of heavily stained extracellular matrix fibers (Fig. 5) which we have found to contain fibronectin using immunoelectron microscopy (see Fig. 10) were often situated in very close transmembraneous apposition to the intracellular actin microfilament bundles. This transmembrane relationship between actin and fibronectin bundles is evidently the ultrastructural correlate of the double-stained acto-fibronectin fibers observed in our immunofluorescence microscopy experiments.

FIBRONEXUSES AT THE MYOFIBROBLAST SURFACE

We observed many fibronexus (FNX)[1]-like transmembrane associations of extracellular fibronectin fibers and cortical 5-nm actin microfilaments localized at the myofibroblast plasma membrane. They appeared to attach the myofibroblasts to each other and to the surrounding extracellular matrix. These FNXs could be grouped into three morphological categories: track-like, plaque-like, and end-on-end (tandem) associations.

TRACK-LIKE FIBRONEXUSES: Railroad track-like associations of parallel bundles of 5-nm actin microfilaments and fibronectin-containing extracellular matrix fibers with an intervening plasma membrane constitute a novel kind of FNX at the myofibroblast surface (Fig. 5; also see Fig. 10 *B*). Track-like FNXs are characterized by relatively long zones of trans-

[1] *Abbreviations used in this paper:* EM, electron microscopy; FNX, fibronexus.

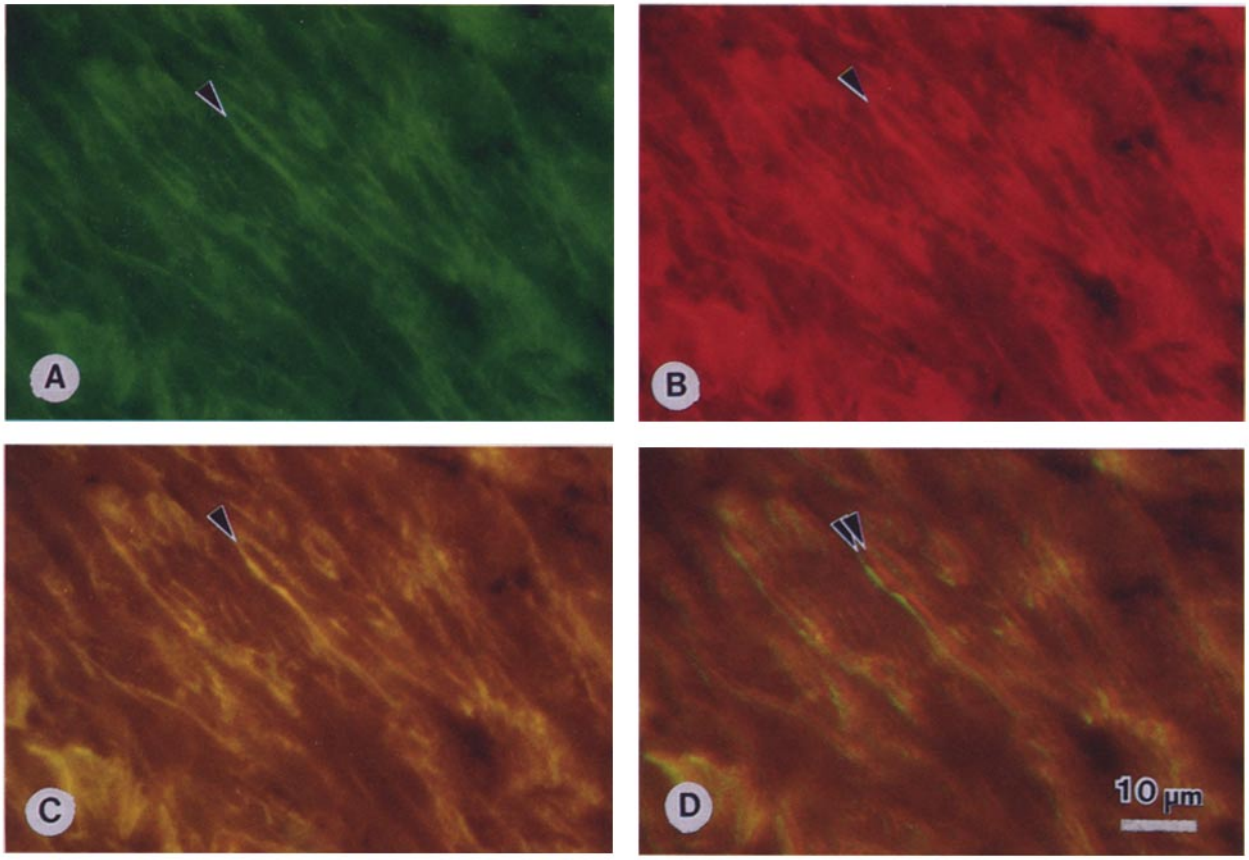

FIGURE 3 Color immunofluorescent micrographs illustrating the high degree of actin-fibronectin coincidence found in 7-d granulation tissue; arrowheads indicate the same fiber. (*A*) Actin pattern seen with fluorescein filters. (*B*) Fibronectin distribution viewed using rhodamine filters. (*C*) Double exposure of the actin pattern in *A* and the fibronectin label in *B* reveals that both types of fibers completely overlap each other (at arrowhead). (*D*) Double exposure similar to that in *C*, which reveals that both the actin and fibronectin labeling of each fiber may be seen as separate entities (at double arrowhead) if the component images are intentionally misaligned. The method is therefore capable of detecting fibronectin and actin fibers that may not be coincident. × 1,000.

membrane interaction ranging in length from ~1 to 2 μm. The intracellular and extracellular components of this FNX are apparently connected by cross-linking fibers that traverse the plasmalemma, and are approximately perpendicular to the longitudinal axis of the cell (Figs. 5, *C* and *D* and 6). These transverse fibers are analogous to the ties of railroad tracks, and are undoubtedly composed of at least three unique elements: a fibronectin-associated portion, a transmembrane part, and an actin-binding component. The degree of closeness between these external and internal linker components can be ascertained from goniometric electron microscope (EM) experiments. If the FNX section is tilted around the longitudinal axes of the linkage fibers (in the plane indicated by the double-headed arrow in Fig. 6*A*), the internal and external components remain co-linear through 30° of tilting (Fig. 6). This observation indicates that the FNX linkage fibers are probably composed of co-axial components rather than non-co-axial superimposed co-linear fibers which might appear co-extensive due to the nature of transmission electron microscopy.

Close associations between collagen fibers and track-like FNXs were also often observed at the myofibroblast surface (Fig. 5*E*), suggesting that complex supramolecular associations between collagen, fibronectin, the plasma membrane, transmembranous linker fibers, and actin microfilaments exist at that surface.

PLAQUE-LIKE FIBRONEXUS: The plaque-like FNX is composed of tufts of densely stained fibronectin fibers ranging from 0.2 to 0.5 μm diam (Fig, 7, *A* and *B–F*; see also 10*D*), associated with submembranous 5-nm actin microfilaments. This type of cell surface complex is similar to the track-like FNX because it also has many transmembrane linkage fibers which appear to connect tufts of extracellular fibronectin with subplasmalemmal actin microfilaments (Fig. 7*A*).

Plaque-like FNXs were usually observed in sections cut parallel to the long axes of the myofibroblasts (direction determined with 1-μm sections). In this orientation, the fibronectin fibers and actin microfilament bundles associated with FNXs were sectioned longitudinally, because the fusiform myofibroblasts were situated parallel to each other (Fig. 4). Therefore, the image of the plaque-like FNX is not simply derived by cross-sectioning through a track-like FNX, since the actin microfilaments of the plaque-like FNXs always exhibited a longitudinal orientation (Fig. 7*A*).

Again via goniometric experiments, we observed that the putative internal and external portions of the transmembranous linker filaments remained co-linear through 20–30° of specimen tilting (Fig. 7, *B–F*), suggesting that they are probably co-axial. In these goniometric studies, a series of 10–12 micrographs, each differing by 10° of tilt, was made for a given FNX. We found that the transmembrane linkage fibers could not be continuously followed for >20–30° of tilting,

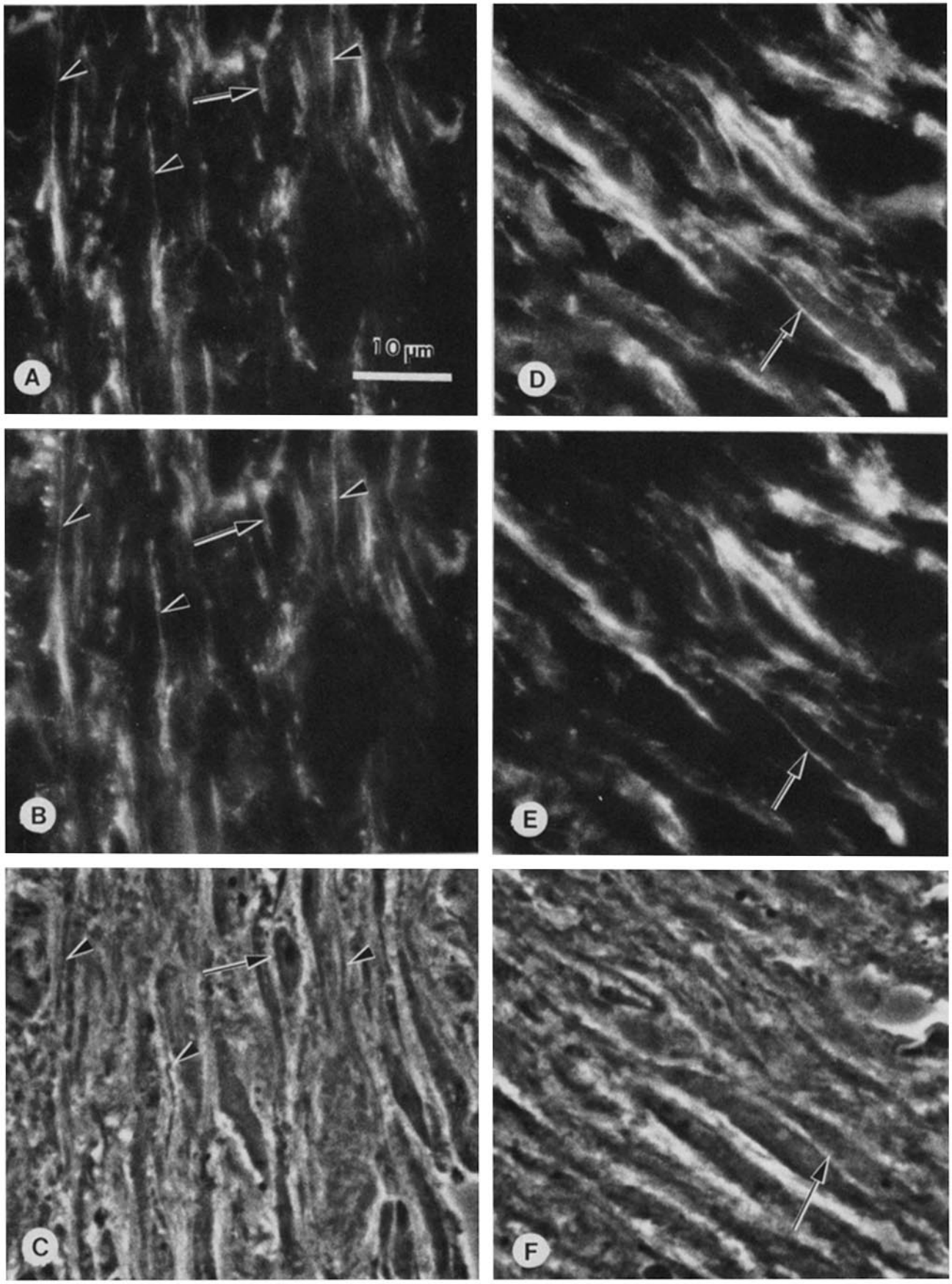

FIGURE 4 Matching double immunofluorescent and phase-contrast micrographs depicting the co-localization of fibronectin (*A* and *D*, rhodamine) and actin (*B* and *E*, fluorescein) fibers on the attenuated myofibroblast processes (arrowheads, *A*–*C*) and at the myofibroblast perimeters (arrows, *A*–*F*). × 1,800.

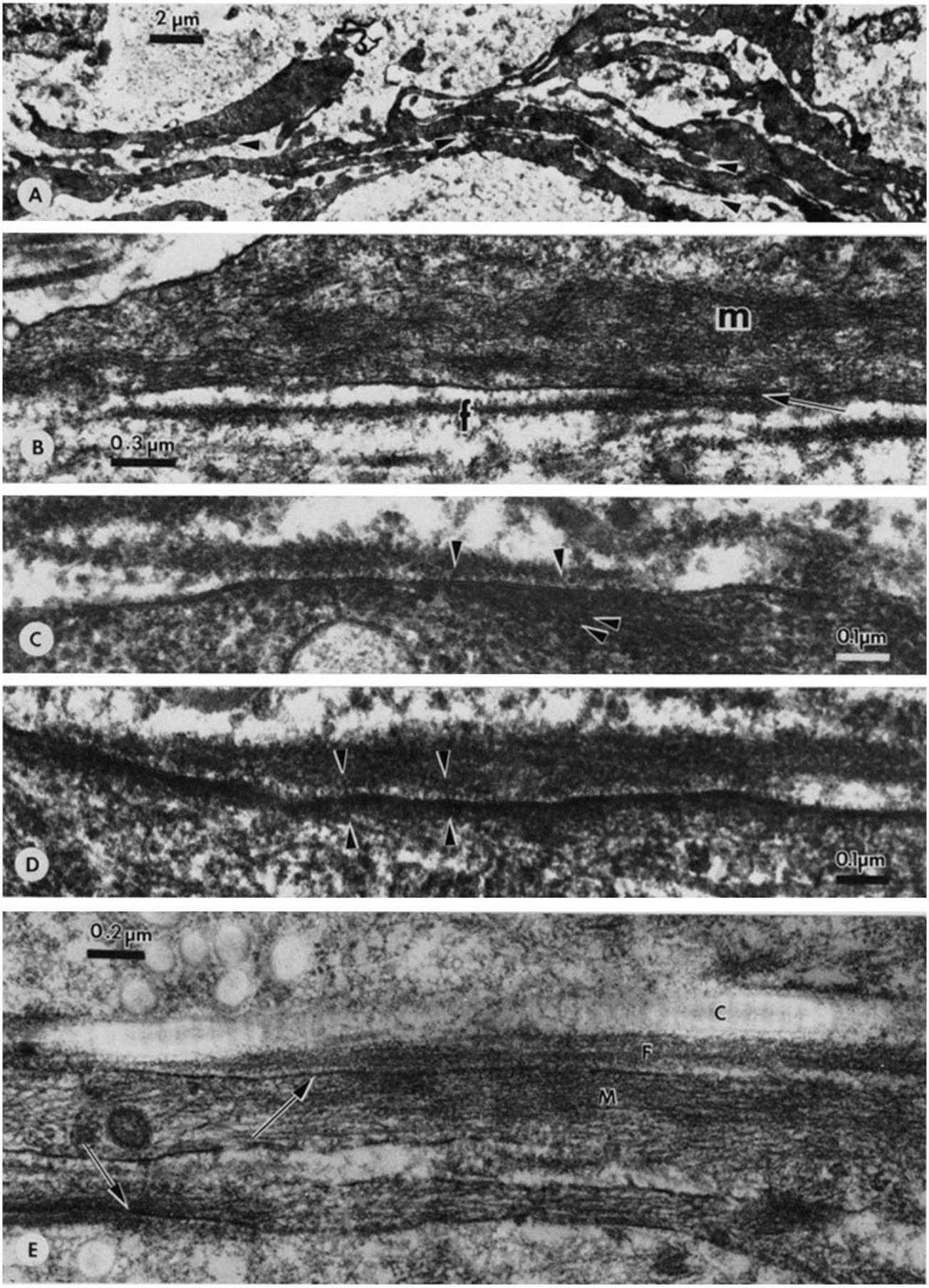
2 μm
A
m
f
B
0.3 μm
C
0.1μm
D
0.1μm
0.2 μm
C
F
M
E

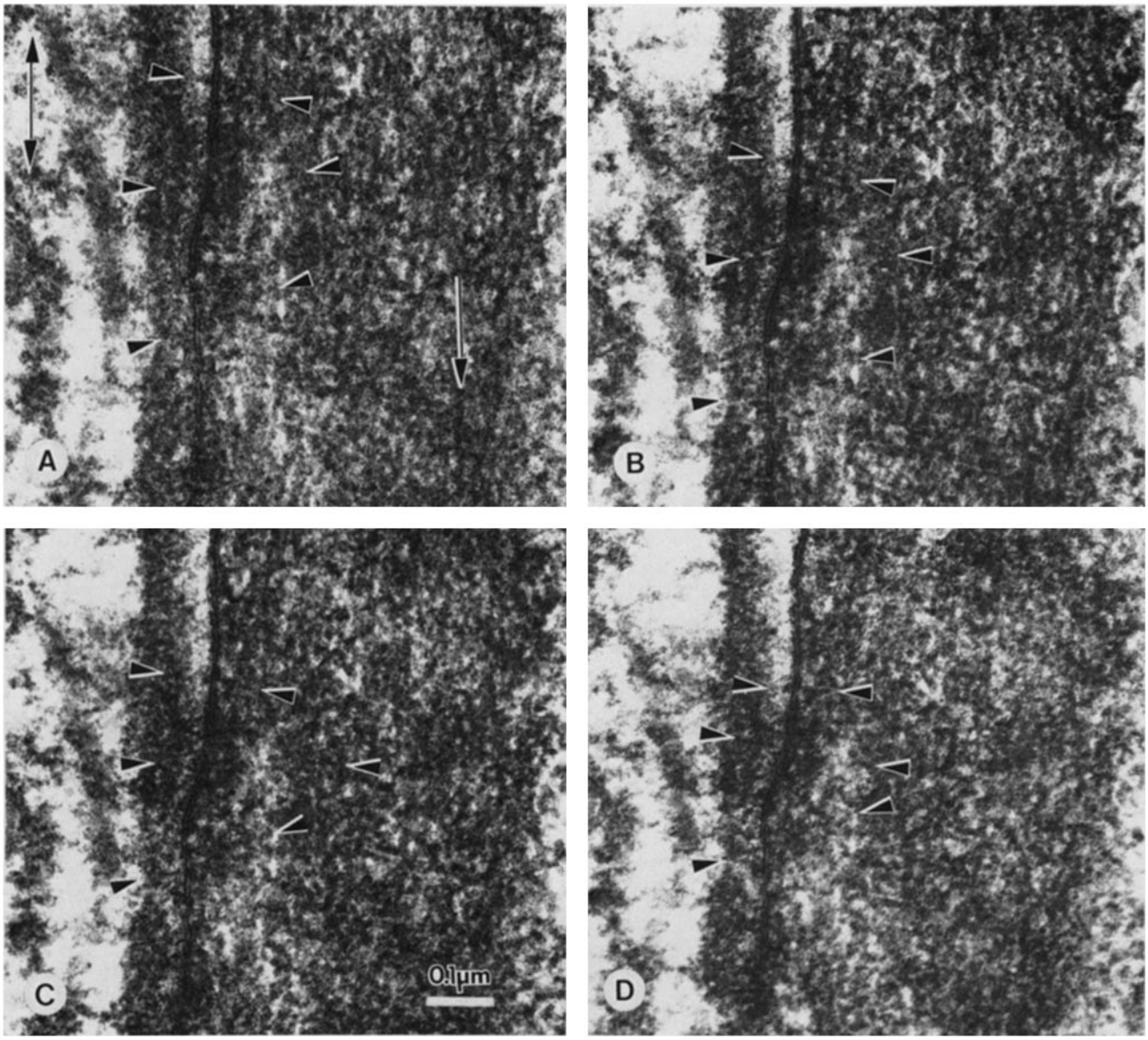

FIGURE 6 Goniometric study of the transmembranous filaments (arrowheads) that apparently link extracellular fibronectin-containing fibers with parallel intracellular 5-nm actin microfilaments (arrow in *A*) at the track-like FNX delineated by the arrow in Fig. 5*B*. The longitudinal axes of the internal and external linkage fiber segments do not separate following 30° of tilting in the orientation shown by the doubleheaded arrow in *A*. (*A*) 20°; (*B*) 30°; (C) 40°; (*D*) 50°. × 100,000.

due to superimposition with high density submembranous material. Therefore, not all of the fibers observed in Fig. 7, *D* and *E* can be seen clearly in every other micrograph of this series. Nevertheless, selected pairs of transmembranous fibers could be resolved in a continuous series of four micrographs (e.g., upper and lower fibers in Fig. 7*B* are also seen in Fig. 7, *C–E*), thus indicating co-linearity for at least 30° of tilt.

TANDEM FIBRONEXUSES: This type of FNX is usually situated at or near the ends of the attenuated myofibroblast cell processes (Figs. 8, 9, and 10, *C* and *D*). It consists of a

FIGURE 5 Electron microscopy of track-like FNXs in plastic sections of 7–9 d guinea pig granulation tissue. (*A*) Low magnification of a cord of elongated myofibroblast cellular processes associated with dense masses of extracellular matrix material (arrowheads). × 5,000. (*B*) A darkly stained 3-μm long fibronectin bundle (*f*) is associated with an actin microfilament cable (*m*) in a track-like fibronexus at its proximal end (arrow). The cross-linking filaments of this FNX region are illustrated in Fig. 6. × 40,500. (*C* and *D*) Numerous transmembranous cross-linking filaments of the track-like FNXs form brush-like arrangements at the plasmalemma. Some of these transmembranous fibers are depicted by the downward- and upward-pointing arrowheads, while 5-nm actin microfilaments are indicated by the leftward-facing arrowheads in C. × 100,000. (*E*) Collagen fibers (*C*) in close lateral apposition to track-like fibronexuses at the plasmalemmata of myofibroblast cell processes. The arrows indicate two track-like FNXs composed of parallel fibronectin-containing fibers (*F*) and actin microfilaments (*M*). × 54,000.

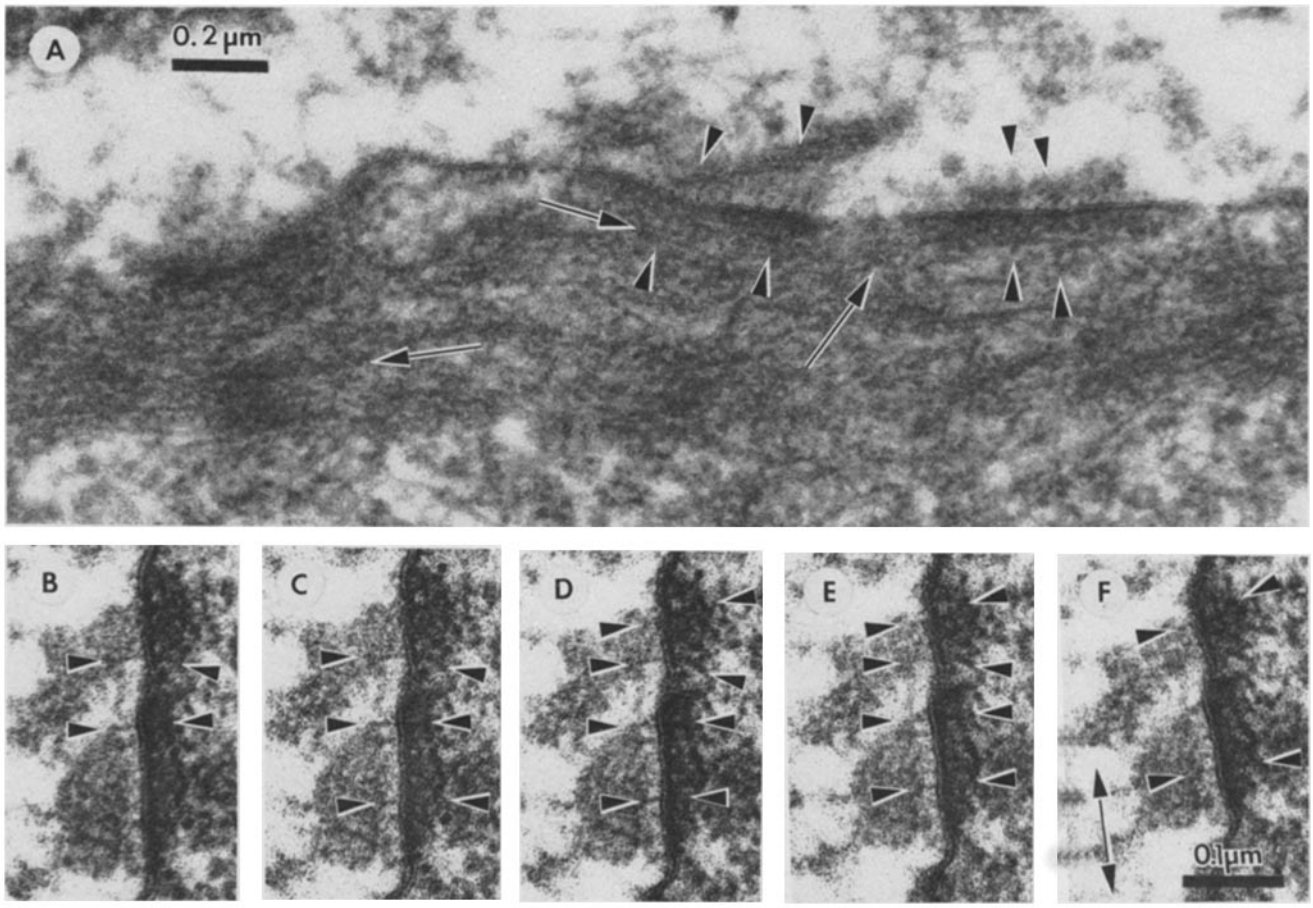

FIGURE 7 Electron microscopy of plaque-like FNXs at the cell surfaces of myofibroblasts in 7–9-d guinea pig granulation tissue. (*A*) Small plaques of cell surface extracellular matrix fibers are associated with an elongated bundle of cortical 5-nm actin microfilaments (arrows) via the many parallel linkage filaments of each FNX (pairs of arrowheads). These cross-linking filaments are oriented normal to the cell membrane and comprised of external (upper arrowheads) and internal (lower arrowheads) segments. (*B–F*) Goniometric analysis of the transmembrane cross-linking filaments of the plaque FNX shows that their extracellular (rightward-facing arrowheads) and intracellular (leftward-facing arrowheads) remain co-linear through 20°–30° of tilting around their longitudinal axes (doubleheaded arrow in *F* indicates the direction of tilt). Corresponding pairs of arrowheads depict the same cross-linking filament after 10° of tilt. (*B*) 0°; (*C*) +10°; (*D*) +20°; (*E*) +30°; (*F*) +40°. (*A*) × 64, 400; (*B–F*) × 131,000.

microfilament bundle and extracellular fibronectin fibers in an end-on-end transmembrane association (Fig. 8 *A* and *B*). On higher magnification, individual 5-nm-diam actin microfilaments and fibronectin-containing fibers of the extracellular matrix appear co-extensive across the plasma membrane (Figs. 8*C* and 9). Goniometric analysis of sections tilted 20–40° about the long axis of the tandem FNX demonstrate that these FNX components are not laterally displaced during tilting (data not shown), strongly suggesting that they are closely associated if not co-extensive. This tandem FNX is very similar to the one we first described for hamster fibroblasts in vitro (42). During those studies many of the FNXs were oriented at small acute angles to the plasmalemma, so that its internal membrane could not be clearly resolved in *en face* sections through the adhesive surface with the goniometer available at that time. Using a high resolution eucentric goniometer capable of high angle tilting, we have now directly visualized the membrane of a tandem FNX which is not seen in the uninclined *en face* section (Fig. 9*A*). If the section is tilted in a direction (double-headed arrow, Fig. 9*B*) to bring the intrafibronexus membrane closer to a cross-sectional orientation, then the intrafibonexus membrane can be observed (arrows, Fig. 9, *B* and *C*) in close association with co-linear FN fibrils and actin microfilaments (arrowheads, Fig. 9, *B* and *C*).

Relative Quantities of Cell Surface Adhesion Sites in Myofibroblasts

In addition to the three varieties of FNXs found in granulation tissue, we also observed that gap junctions were present at the myofibroblast surfaces. Since the gap junction has already been reported to be an intercellular attachment site in granulation tissue (12), it became necessary to ascertain the relative distributions of these various cellular adhesion sites within this tissue. These results are presented in Table I. The data show that approximately equal quantities of plaque, tandem, and track FNXs were present in the sections sampled. However, only 4% of the total sample of cell-surface adhesion sites were gap junctions.

Immunoelectron Microscopy of Granulation Tissue Fibronexuses

An immunoelectron microscopic study of fibronectin labeling upon ultrathin cryosections of granulation tissue was also performed using a biotin-avidin labeling protocol, as well

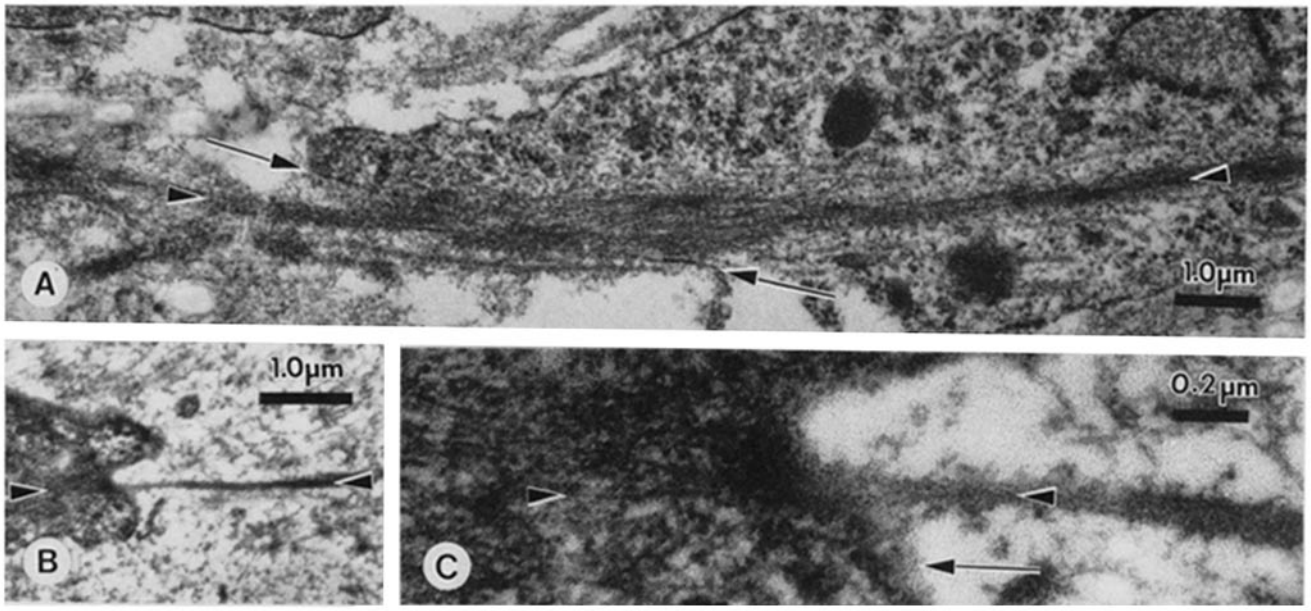

FIGURE 8 Tandem fibronexuses located at the ends of attenuated myofibroblast cell processes. (*A*) A cluster of densely stained extracellular matrix fibers (arrowhead at left) forms an end-on-end association with an actin microfilament bundle (arrowhead at right) across the plasmalemma (arrows). × 11,600. (*B*) Another tandem FNX comprised of extracellular matrix fibers (right arrowhead) and a bundle of actin microfilaments (left arrowhead). × 12,500. (*C*) Higher magnification of the tandem fibronexus in *B* depicting the individual extracellular fibronectin fibers (right arrowhead) which are co-extensive with 5-nm actin microfilaments (left arrowhead) across the obliquely sectioned cell membrane (arrow). × 51,500.

as microtomy and staining techniques modified from methods developed by Tokuyasu (48, 49). In this way we were able to confirm that the dense extracellular fibrous component of the various FNXs found at the myofibroblast surface is rich in fibronectin (Fig. 10). Although cortical microfilaments are visible with this method (arrowheads in Fig. 10, *A*, *C*, and *D*), they are much more discernible with standard EM techniques. Consequently, it is beneficial to compare these immunoelectron micrographs with corresponding plastic sections through the FNX.

In these cryosections, dense masses of antifibronectin-labeled material were often observed at the external surface of the myofibroblast plasmalemma, which could be recognized easily when seen in transverse section. Delicately stained 5-nm actin microfilaments could also be found immediately beneath this cell membrane (arrowheads Fig. 10*A*). Examples of fibronexuses that closely resemble the three kinds of FNXs seen in plastic-embedded material were also observed. Track-like FNXs, in which elongated masses of immunofibronectin-labeled material were closely associated with the cell surface and cortical microfilament bundles for 1-μm or more, were found in lateral apposition to collagen fibers (compare Fig. 10*B* with Fig. 5*E*). Linear felt-like mats of immunoferritin-labeled fibronectin were also found in end-on end association with the tips of attenuated myofibroblast cellular processes (Fig. 10, *C* and *D*). These processes are filled with actin (shown by immunofluorescence microscopy in Fig. 4, *A–C*), bundles of 5-nm microfilaments (observed by electron microscopy of epon sections in Figs. 8 and 9), and finely stained microfilaments seen in ultrathin cryosections (arrowheads, Fig. 10, *C* and *D*). Therefore, these complexes constitute tandem FNXs (compare Figs. 10*C* and 8*A* and Figs. 10*D* and 9*A*). In addition, plaque-like FNXs with ~0.4-μm-diam tufts of immunofibronectin-stained material were seen at the cell surface (compare Figs. 10*D* and 7*A*). Throughout these experiments, the immunoferritin labeling for fibronectin was highly localized on the dense extracellular material at the cell surface, and abruptly stopped at the plasmalemma (Fig. 10, *A–D*). All buffer and nonimmune rabbit IgG controls exhibited low levels of background, and in particular, the specific immunofibronectin staining was blocked by preincubation with excess purified fibronectin (Fig. 10*E*).

DISCUSSION

Our immunofluorescent micrographs produced by double labeling 1-μm semithin frozen sections of guinea pig granulation tissue show an extensive co-distribution of actin and fibronectin in fibers at the surfaces of its myofibroblasts. Although some actin fibers were either not fibronectin associated, or found to be closely associated with fibronectin along only a portion of their entire length, the overwhelming majority of fibers were double stained for actin and fibronectin, as demonstrated by color double exposures. These apparent acto-fibronectin fibers were localized at the perimeters of the myofibroblasts, and along their long attenuated processes which extend from either end of the cell outward into the surrounding extracellular matrix. With double-label immunofluorescence microscopy, we often observed acto-fibronectin fibers apparently isolated with the extracellular matrix, seemingly unattached to myofibroblasts (Fig. 4, *A–C*). Presumably, these double-stained fibers are the longitudinally sectioned myofibroblast processes that contain compact actin-microfilament bundles, and are associated with densely stained fibronectin-containing extracellular matrix fibers seen with EM (Figs. 5 and 10*C*). Thus, the production of 1-μm semithin cryosections using EM methods (49) has improved the resolution of granulation tissue immunofluorescence micrographs to the point where much more detail of the fibronectin and actin staining patterns can be seen than in previous light microscopic studies (7, 14). This co-distribution of actin

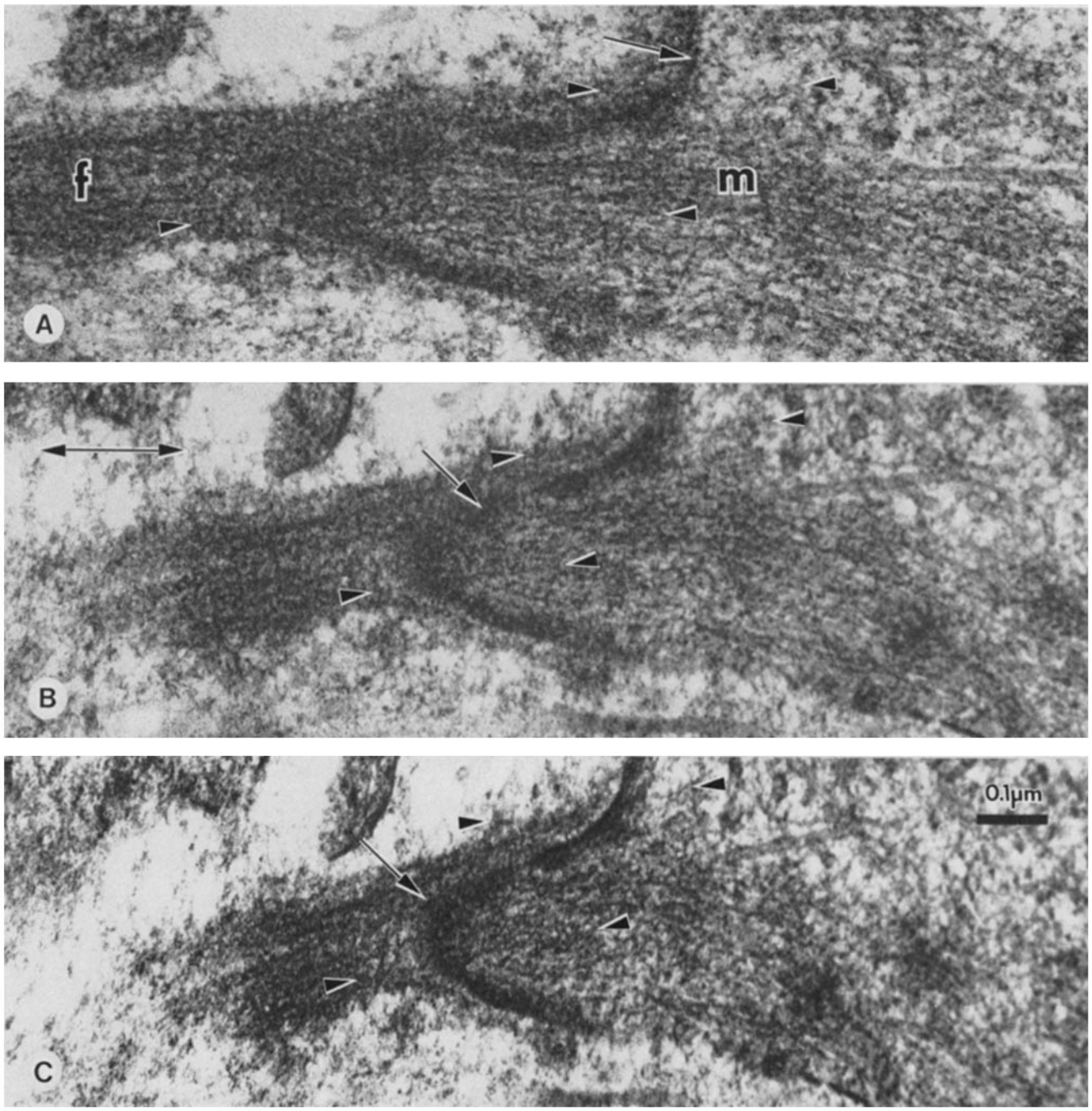

FIGURE 9 Goniometry of a tandem fibronexus (*A*) comprised of external fibronectin fibers (*f*) and intracellular actin microfilaments (*m*). This series of electron micrographs demonstrates that the plasmalemma (arrows) within this FNX may be seen at the tip of the myofibroblast process (arrow in C) by tilting the specimen in the direction indicated by the double arrow in *B*. Corresponding pairs of arrowheads depict actin microfilaments (arrowheads at right) and fibronectin fibers (arrowheads at left) which remain co-linear from 0° to a 60° tilt. (*A*) 0°; (*B*) 50°; (C) 60°. × 111,000.

and fibronectin in granulation tissue indicated to us that fibronexuses might be present at the myofibroblast surface in vivo. Therefore, we studied this tissue with structural EM (plastic sections) and immunoelectron microscopy (ultrathin cryosections) to test this hypothesis, and to clarify the structure of the acto-fibronectin fibers seen with immunofluorescence microscopy. We found that these apparently unitary fibers are actually comprised of closely apposed actin and fibronectin filaments plus an intervening plasma-membrane when observed with EM. Our electron micrographs also firmly establish that the FNX is a widespread adhesive structure of the myofibroblast surface in guinea pig granulation tissue. These results further extend our in vitro studies of the fibroblast FNX (42–44, 46), to the tissue level in vivo, and strongly suggest that it is an important adhesive complex within granulation tissue.

The close coincidence of most of the actin bundles with fibronectin fibers demonstrated by our immunofluorescent micrographs of granulation tissue is due to a number of factors. Hamster, rat, and human fibroblasts exhibit a close co-distribution of fibrillar fibronectin arrays and actin bundles in most cells studied in vitro (22, 26, 27, 42, 43). This close

relationship between the actin-cytoskeleton and the fibronectin-containing extracellular matrix is apparently a property of differentiated fibroblasts grown in vitro, which is maximized when the cells are growth arrested, immobile, and well spread upon the substratum (27, 43, 46). Since myofibroblasts are a well-differentiated type of fibroblast, one might likewise expect them to show a high degree of actin-fibronectin coincidence, which is indeed the case in guinea pig granulation tissue. The observation that most of the myofibroblast actin bundles exhibit coincident fibronectin staining may also be explained on the basis of their specialized cell shape. The myofibroblast cytoplasm is not spread out into an extensive sheet like that observed during growth arrest in tissue culture, but instead is attenuated into a very long, thin bipolar shape in the granulation tissue. Under these circumstances, most of the actin microfilament bundles are situated in close apposition to the plasmalemma in the cytoplasmic cortex and elongated processes (Fig. 5). Unlike the in vitro situation where bundles of actin microfilaments may also be separated from the surface membrane (18), the actin-bundles of granulation tissue myofibroblasts usually appear to be surface localized, where they may interact with putative membrane-bound receptors of the FNX complex (43, 44) for nearly their entire length.

During our ultrastructural analysis of dermal granulation tissue, we found that three unique types of FNXs are localized at the myofibroblast surface membrane. In addition to the tandem or end-on-end FNX observed previously in vitro (42), we also saw track-like and plaque-like FNXs which are novel structures that differ greatly from tandem FNXs. The plaque and track-like FNXs may be distinguished via the size of their extracellular fibronectin-containing component. The fibronectin fibers of the plaque-like FNX comprise a tuft that is <0.5 μm long, whereas the track-like FNX contains an elongated fibronectin bundle that is >1.0 μm long. The latter two types of FNXs are similar in that they are both composed of parallel sets of fibronectin and actin fibers connected by perpendicular transmembranous linker fibers. The exact chemical nature of these linkage fibers is unknown, but one may hypothesize that they are composed of at least three elements: (*a*) a hydrophilic external portion attaching the fibronectin and often the overlying collagen fibers to the cell surface, (*b*) a cluster of hydrophobic intramembranous components which serves as a bivalent receptor for both co-axial extracellular and intracellular linkage fibrils, and (*c*) a hydrophilic intracytoplasmic element which attaches the 5-nm actin microfilaments, perhaps via vinculin (5, 15, 43, 46), to the intramembranous receptor. These linear linkage components are closely apposed and probably co-axial across the cell membrane as shown by our extensive goniometric analysis of 61 plaque and track FNXs, in which the extracellular and cytoplasmic components remained co-extensive through a 20–30° tilt. The internal actin-associated section of the linkage fibril is morphologically, functionally, and possibly chemically similar to the lateral 110-kdalton thread-like connections between actin microfilament bundles and the cell membrane of intestinal microvilli, and within inner ear hair cell stereocilia (24, 32–34). Also, a newly described 140-kdalton integral membrane glycoprotein that is tightly associated with the cytoskeleton of the intestinal microvillus (9) is functionally analogous to the intramembranous component of the FNX, since both molecules might provide an attachment site for the lateral bridging of actin microfilaments to the cell membrane. However, the exact chemical relationship, if any, between these molecules and their putative analogues within the FNX is unknown at present, and awaits a detailed biomolecular dissection of the FNX.

The fibronexus may also be analyzed from a structural engineering viewpoint. If the actin and fibronectin components of the FNX equal the adherends of a joint, and if the intermediate cross-linking fibers and transmembranous ligands represent the adhesive that binds them together, the FNX may be thought of as an adhesive joint. Such joints may be lap joints, in which linkage elements are directed perpendicular to the planes of the overlapping fibers, or butt joints where two linear adherends are joined end-on-end (3). Generally speaking, lap joints have a high sheer stress component, and are much more stable than butt joints characterized by dominant tensile stress components (3). Since track and plaque-like FNXs are analogous to lap joints, and tandem FNXs are similar to the adhesively weaker butt joints, one would conclude that the former FNX types are the most mechanically stable. If this assumption is correct, it is very likely that the track-like and plaque-like FNXs are responsible for most of the cohesion of granulation tissue since they constitute two-thirds of the FNXs observed.

In their studies of rat and rabbit dermal granulation tissue, Gabbiani et al. (12) observed that gap junctions were present between the myofibroblast cell processes. We have confirmed this observation in our experiments, but have also determined that gap junctions make up only 4% of the total population of cell surface myofibroblast adhesion sites in granulation tissue. Based on their sparse numbers, it is unlikely that gap junctions play a major role in granulation tissue cohesion. Because the FNX appears to be the most common form of binding site attaching myofibroblasts to each other and to the extracellular matrix of granulation tissue, we think that it is the organelle primarily responsible for the cohesion of this tissue. The gap junctions are probably responsible for the metabolic coupling of the myofibroblasts (17), and perhaps for the synchronization of their contraction (12). Gabbiani and co-workers (13, 14) also described a well-defined layer of "basal lamina" material associated with dense microfilament bundles at the myofibroblast cell membrane. We believe that this complex is an FNX because of its structural similarity to the track-like FNXs described here. It is probably not appropriate to refer to this material as a basal lamina since that terminology would lead to confusion with the basement membrane that is characteristic of epithelial and endothelial cells (28). The FNXs we observed are definitely not basement membranes for the following reasons: (*a*) basement membranes form a thin *continuous* meshwork of randomly arranged fibrils at the basal surfaces of epithelial, endothelial, and various glandular cells, but not fibroblasts (28, 36, 50); (*b*) the lamina densa of the basement membrane is separated from the basal cell membrane by an electron-lucent lamina lucida of uniform thickness, whereas: (i) the fibronectin component of the FNXs does not continuously coat the cell surface (Fig. 7), (ii) the bundles of fibronectin fibers that are involved in track-FNXs approach the cell membrane at a small acute angle and are only engaged in a transmembrane association near their termini (Fig. 5), (iii) the transmembrane linkage fibers of the FNX are more numerous and more densely stained that the fibers of the lamina lucida, and (iv) tandem FNXs are obviously not basement membranes.

The conspicuous presence of acto-fibronectin fibers in our

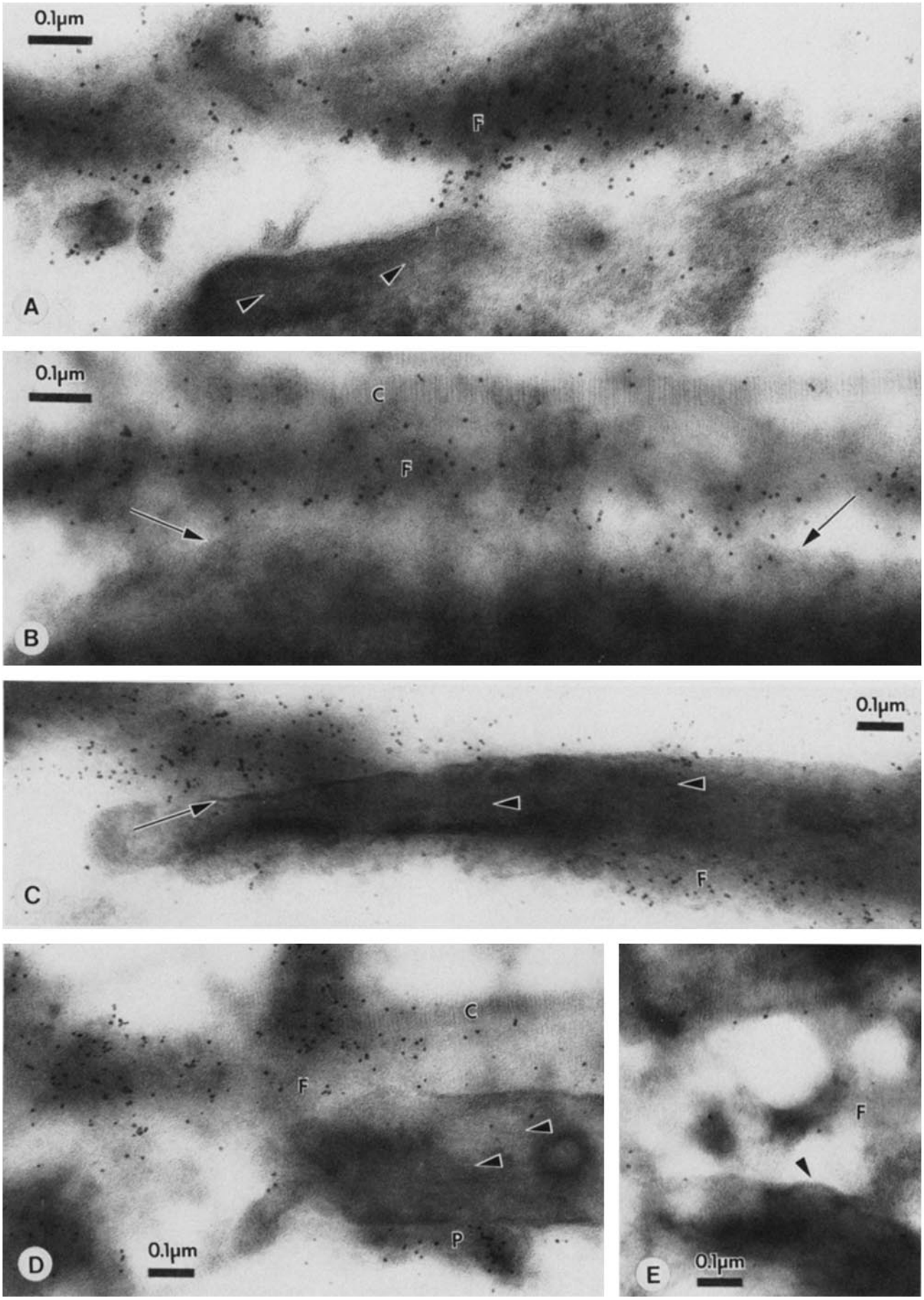
0.1μm
F
A
0.1μm
C
F
B
0.1μm
C
F
0.1μm
C
F
P
D
F
0.1μm
E

TABLE I

Relative Distribution of FNXs and Gap Junctions in Guinea Pig Granulation Tissue

Attachment site	Number*	Percentage
Plaque-like FNX	26	28.9
Tandem FNX	25	27.8
Track-like FNX	35	38.9
Gap junction	4	4.4

* 22 blocks of 7-9-d dermal granulation tissue (~1 mm^3) were ultrathin sectioned and at least two grids were studied for each block. Each FNX scored had co-axial transmembrane linkage fibers as determined by goniometric analysis.

immunofluorescent micrographs of guinea pig granulation tissue strongly suggests that the fibronexus is a dominant adhesive complex at the myofibroblast surface, and our ultrastructural studies of this tissue support this conclusion. Therefore, the fibronexus is not only an important cell surface structure utilized by fibroblasts for substrate adhesion in vitro, (6, 22, 26, 27, 35, 42–44, 46), but it also apparently plays a functionally important role in the formation and cohesion of granulation tissue in vivo. This notion is supported by several time-course studies of experimental granulation tissue in which the appearance of fibronectin matrix occurs early, concurrent with fibrin clot formation, and again a few days later at the time of fibroblast invasion, before the synthesis of interstitial collagens (19, 25, 30). Fibronectin fragments have been shown to be chemotactic for fibroblasts in vitro (37), and thus the fibronectin-rich clot probably induces early fibroblast migration into the wound area. As the dermal fibroblasts grow into the wound on this early extracellular scaffold, they evidently elaborate more conspicuous actin-microfilament bundles than those observed in ordinary fibroblasts (14). Fibronectin undoubtedly is a primary agent in this process since it has been found to increase cellular alignment (56), stimulate actin-microfilament bundle formation (2, 53), and to induce early fibronexus morphogenesis in transformed fibroblasts (44). These experiments suggest that the binding of fibronectin to the plasma membranes of fibroblasts that enter the wound causes fibronexus formation and the subsequent generation of prominent actin microfilament bundles. During the later stages of the healing process, collagenous proteins are also deposited onto the fibronectin-containing scaffold and gradually become the dominant extracellular matrix protein of the granulation tissue (30). Since we observed that FNXs are closely associated with collagen fibers situated along the myofibroblast processes (Fig. 5 *E* and 10, *B* and *D*), it is very probable that at this stage, fibronectin and the fibronexus function to tether the myofibroblasts to each other and to the extracellular collagen. Fibronectin is ideally suited to perform this function because the fibronectin molecule is composed of several domains, which are regionally specific receptors for collagen, gelatin, and the cell surface, among other substances (21, 40, 41, 52). Our in vivo results agree with the in vitro observations from several laboratories that have reported an extensive co-distribution of collagen and fibronectin (4, 10, 31, 51). In addition, our direct in vivo visualization of fibronectin-mediated connections between collagen, the plasma membrane, and the actin cytoskeleton strongly suggests that fibronectin is a dominant ligand molecule of connective tissue. Thus, fibronectin and the fibronexus might not only govern fibroblast adhesion and metabolism in early granulation tissue, but probably also serve as important mediators of cohesion in more mature granulation tissue which is synthesizing collagen (25, 30). The fibronexus may also serve to transmit the collective forces generated by the contraction of actin microfilaments within myofibroblasts throughout the granulation tissue, and thereby affect wound constriction. In fact, these forces may have contributed to the extensive co-alignment of actin and fibronectin fibers that we observed in granulation tissue.

The authors are grateful to Drs. K. T. Tokuyasu and S. J. Singer for excellent instruction in the production and immunolabeling of ultrathin frozen sections, to Dr. J. Whitehead of Vector Laboratories for helpful discussions on the use of avidin-ferritin conjugates, to Dr. Jim J. C. Lin of the Cold Spring Harbor Laboratories for generously providing his monoclonal actin antibodies for this study, to John J. Kath for help with the color photography, and to Marilyn M. Serson for her excellent secretarial skills.

This work was partially supported by grants from the National Institutes of Health to I. I. Singer (National Cancer Institute grant No. RO1CA27389-03) and to R. A. F. Clark (AM 31514-01).

Received for publication 11 October 1983, and in revised form 2 February 1984.

REFERENCES

1. Ainsworth, S. K., and M. J. Karnovsky. 1972. An ultrastructural staining method for enhancing the size and electron opacity of ferritin in thin sections. *J. Histochem. Cytochem.* 20:225–229.
2. Ali, I. U., V. Mautner, R. Lanza, and R. O. Hynes. 1977. Restoration of normal morphology: adhesion and cytoskeleton in transformed cells by addition of a transformation-sensitive surface protein. *Cell.* 11:115–126.
3. Bickerman, J. J. 1968. The Science of Adhesive Joints. Academic Press, Inc., New York. Second ed. 229 pp.
4. Bornstein, P., and J. F. Ash. 1977. Cell surface associated structural proteins in connective tissue cells. *Proc. Natl. Acad. Sci. USA.* 74:2480–2484.
5. Burridge, K., and J. R. Feramisco. 1980. Microinjection and localization of a 130K

FIGURE 10 Antifibronectin immunoferritin labeling on ultrathin cryosections of the myofibroblast surface, stained with the biotin/avidin method and biotinylated ferritin as described in Materials and Methods. (*A*) Darkly stained masses of extracellular matrix (*F*) contain abundant fibronectin antigens and are closely associated with the crosscut cell membrane and underlying 5-nm actin microfilaments (arrowheads). × 114,000. (*B*) Example of a track-like fibronexus closely apposed to a collagen fiber (C); compare with Fig. 5 *E*. The longitudinal immunolabeled fibronectin fiber (*F*) interacts with ~1 μm of obliquely sectioned cell membrane (between arrows). × 114,000. (*C*) A tandem fibronexus (arrow) located near the terminus of an attenuated myofibroblast process containing actin microfilaments (arrowheads); compare with Fig. 8*A* which depicts a plastic section of a similar FNX. Fibronectin antigens are concentrated in the outer FNX components (above arrow), and along the obliquely cut plasmalemma (*F*). × 84,000. (*D*) This cryosection exhibits another fibronectin-rich (*F*) tandem fibronexus that interacts with a collagen fiber (C) at the tip of a myofibroblast cell process containing microfilaments (arrowheads); compare with micrograph of a corresponding plastic section in Fig. 9*A*. A plaque-like fibronexus (*P*), similar to those in Fig. 7*A*, is also visible at the lower cell surface × 84,000. (*E*) Control ultrathin cryosection stained as above with fibronectin antibodies that were pretreated with excess purified chick embryo fibroblast fibronectin. Only a very sparse ferritin background is present on the extracellular fibers (*F*) located at the myofibroblast surface (arrowhead). × 84,000.

protein in living fibroblasts: a relationship to actin and fibronectin. *Cell.* 19:587–595.
6. Chen, W.-T., and S. J. Singer. 1982. Immunoelectron microscopic studies of the sites of cell-substratum and cell-cell contacts in cultured fibroblasts. *J. Cell Biol.* 95:205–222.
7. Clark, R. A. F., P. DellaPelle, E. Manseau, J. M. Lanigan, H. F. Dvorak, and R. B. Colin. 1982. Blood vessel fibronectin increases in conjunction with endothelial cell proliferation and capillary ingrowth during wound healing. *J. Invest. Derm.* 79:269–276.
8. Clark, R. A. F., H. F. Dvorak, and R. B. Colvin. 1981. Fibronectin in delayed-type hypersensitivity skin reactions: associations with vessel permeability and endothelial cell activation. *J. Immunol.* 126:787–793.
9. Coudrier, H., H. Reggio, and D. Louvard. 1983. Characterization of an integral membrane glycoprotein associated with the microfilaments of pig intestinal microvilli. *EMBO (Eur. Mol. Biol. Organ.) J.* 2:469–475.
10. Furcht, L. T., D. Smith, G. Wendelschafter-Crabb, D. V. Mosher, and J. M. Foidart. 1980. Fibronectin presence in native collagen fibrils of human fibroblasts: immunoperoxidase and immunoferritin localization. *J. Histochem. Cytochem.* 28:1319–1333.
11. Gabbiani, G. 1979. The role of contractile proteins in wound healing and fibrocontractive diseases. *Methods Achiev. Exp. Pathol.* 9:187–206.
12. Gabbiani, G., C. Chaponnier, and I. Huttner. 1978. Cytoplasmic filaments and gap junctions in epithelial cells and myofibroblasts during wound healing. *J. Cell. Biol.* 76:561–568.
13. Gabbiani, G., B. J. Hirschel, G. B. Ryan, P. R. Statkov, and G. Majno. 1972. Granulation tissue as a contractile organ. A study of structure and function. *J. Exp. Med.* 135:719–734.
14. Gabbiani, G., and D. Montandon. 1977. Reparative processes in mammalian wound healing: the role of contractile phenomena. *Int. Rev. Cytol.* 48:187–219.
15. Geiger, B. 1979. A 130K protein from chicken gizzard: its localization at the termini of microfilament bundles in cultured chicken cells. *Cell.* 18:193–205.
16. Giloh, H., and J. W. Sedat. 1982. Fluorescence microscopy: reduced photobleaching of rhodamine and fluorescein protein conjugates by n-propyl gallate. *Science (Wash. DC).* 217:1252–1255.
17. Gilula, N. B., O. R. Reeves, and A. Steinbach. 1972. Metabolic coupling, ionic coupling and cell contacts. *Nature (Lond.).* 235:262–265.
18. Goldman, R. D., B. Chojnacki, and M.-J. Yerna. 1979. Ultrastructure of microfilament bundles in baby hamster kidney (BHK-21) cells. *J. Cell. Biol.* 80:759–768.
19. Grinnell, F., R. E. Billingham, and L. Burgess. 1981. Distribution of fibronectin during wound healing. *J. Invest. Derm.* 76:181–189.
20. Grinnell, F., and M. K. Feld. 1979. Initial adhesion of human fibroblasts in serum-free medium: possible role of secreted fibronectin. *Cell.* 17:117–129.
21. Hayashi, M., and K. M. Yamada. 1981. Differences in domain structures between plasma and cellular fibronectins. *J. Biol. Chem.* 256:11292–11300.
22. Heggeness, M. H., J. F. Ash, and S. J. Singer. 1978. Transmembrane linkage of fibronectin in intracellular actin-containing filaments in cultured human fibroblasts. *Ann. NY Acad. Sci.* 312:414–417.
23. Herman, I. M., N. J. Crisona, and T. D. Pollard. 1981. Relation between cell activity and the distribution of cytoplasmic actin and myosin. *J. Cell Biol.* 90:84–91.
24. Hirokawa, N., and L. G. Tilney. 1982. Interactions between actin filaments and between actin filaments and membranes in quick-frozen and deeply etched hair cells of the chick ear. *J. Cell Biol.* 85:249–261.
25. Holund, B., I. Clemmensen, P. Junker, and H. Lyon. 1982. Fibronectin in experimental granulation tissue. *Acta Pathol. Microbiol. Scand. Sect. C Immunol.* 90:159–165.
26. Hynes, R. O., and A. T. Destree. 1978. Relationships between fibronectin (LETS protein) and actin. *Cell.* 15:875–886.
27. Hynes, R. O., A. T. Destree, and D. D. Wagner. 1982. Relationships between microfilaments, cell-substratum adhesion, and fibronectin. *Cold Spring Harbor Symp. Quant. Biol.* 46:659–670.
28. Kefalides, N. A., R. Alper, and C. C. Clark. 1979. Biochemistry and metabolism of basement membranes. *Int. Rev. Cytol.* 61:167–228.
29. Klebe, R. J. 1974. Isolation of a collagen dependent cell attachment factor. *Nature (Lond.).* 250:248–251.
30. Kurkinen, M., A. Vaheri, P. J. Roberts, and S. Stenman. 1980. Sequential appearance of fibronectin and collagen in experimental granulation tissue. *Lab. Invest.* 43:47–51.
31. Little, C. D., and W.-T. Chen. 1982. Masking of extracellular collagen and the codistribution of collagen and fibronectin during matrix formation by cultured embryonic fibroblasts. *J. Cell Sci.* 55:35–50.
32. Matsudaira, P. T., and D. R. Burgess. 1979. Identification and organization of the components in the isolated microvillus cytoskeleton. *J. Cell Biol.* 83:667–673.
33. Mooseker, M. S., and L. G. Tilney. 1975. Organization of an actin filament-membrane complex. Filament polarity and membrane attachment in the microvilli of intestinal epithelial cells. *J. Cell Biol.* 67:725–743.
34. Mukherjee, T. M., and L. A. Staehelin. 1971. The fine structural organization of the brush border of intestinal epithelial cells. *J. Cell. Sci.* 8:573–599.
35. Pfeffer, L. M., E. Wang, and I. Tamm. 1980. Interferon effects on microfilament organization, cellular fibronectin distribution, and cell motility in human fibroblasts. *J. Cell. Biol.* 85:9–17.
36. Pitelka, D. R., S. T. Hamomoto, and B. N. Taggart. 1980. Basal lamina and tissue recognition in malignant mammary tumors. *Cancer Res.* 40:1600–1611.
37. Postlewaite, A. E., J. Keksi-Oja, G. Balian, and A. H. Kang. 1981. Induction of fibroblast chemotaxis by fibronectin: localization of the chemotactic region to a 140,000-molecular weight non-gelatin-binding fragment. *J. Exp. Med.* 153:494–499.
38. Repesh, L. A., T. J. Fitzgerald, and L. T. Furcht. 1982. Fibronectin involvement in granulation tissue and wound healing in rabbits. *J. Histochem. Cytochem.* 30:351–358.
39. Reynolds, E. S. 1963. The use of lead citrate at high pH as an electron opaque stain in electron microscopy. *J. Cell Biol.* 17:208–219.
40. Ruoslahti, E., E. G. Hayman, E. Engvall, W. C. Cothran, and W. T. Butler. 1981. Alignment of biologically active domains in the fibronectin molecule. *J. Biol. Chem.* 256:7277–7281.
41. Sekiguchi, K., and S. Hakomori. 1980. Functional domain structure of fibronectin. *Proc. Natl. Acad. Sci. USA.* 77:2661–2665.
42. Singer, I. I. 1979. The fibronexus: a transmembrane association of fibronectin-containing fibers and bundles of 5 nm microfilaments in hamster and human fibroblasts. *Cell.* 16:675–685.
43. Singer, I. I. 1982. Association of fibronectin and vinculin with focal contacts and stress fibers in stationary hamster fibroblasts. *J. Cell Biol.* 92:398–408.
44. Singer, I. I. 1982. Fibronexous formation is an early event during fibronectin-induced restoration of more normal morphology and substrate adhesion patterns in transformed hamster fibroblasts. *J. Cell Sci.* 56:1–20.
45. Singer, I. I., D. W. Kawka, D. M. Kazazis, E. T. Dobi, and R. A. F. Clark. 1983. Immunoelectron microscopic localization of the fibronexis at the cell surface of granulation tissue myofibroblasts. *J. Cell Biol.* 97(5, Pt. 2):123*a*. (Abstr.)
46. Singer, I. I., and P. R. Paradiso. 1981. A transmembrane relationship between fibronectin and vinculin (130KD protein): serum modulation in normal and transformed hamster fibroblasts. *Cell.* 24:481–492.
47. Ternynck, T., and S. Avrameas. 1976. Polymerization and immobilization of proteins using ethylchloroformate and glutarldehyde. *Scand. J. Immunol. Suppl.* 3:29–35.
48. Tokuyasu, K. T. 1980. Adsorption staining method for ultrathin frozen sections. *In* Proceedings of 38th meeting of electron miscroscopy society of America. G. W. Bailey, editor. Claitor, Baton Rouge, LA. 760–763.
49. Tokuyasu, K. T. 1980. Immunocytochemistry on ultrathin frozen sections. *Histochem. J.* 12:381–403.
50. Vaccaro, C. A., and J. S. Brody. 1981. Structural features of alveolar wall basement membrane in the adult rat lung. *J. Cell Biol.* 91:427–437.
51. Vaheri, A., M. Kurkinen, V. P. Lehto, E. Linder, and R. Timpl. 1978. Codistribution of pericellular matrix proteins in cultured fibroblasts and loss in transformation: fibronectin and procollagen. *Proc. Natl. Acad. Sci. USA.* 75:4944–4948.
52. Wagner, D. D., and R. O. Hynes. 1980. Topological arrangement of the major structural features of fibronectin. *J. Biol. Chem.* 255:4304–4312.
53. Willingham, M. C., K. M. Yamada, S. S. Yamada, J. Pouyssegur, and I. Pastan. 1977. Microfilament bundles and cell shape are related to adhesiveness to substratum and are dissociable from growth control in cultured fibroblasts. *Cell.* 10:375–380.
54. Wood, G. S., and R. Warnke. 1981. Suppression of endogenous avidin-binding activity in tissues and its relevance to biotin-avidin detection systems. *J. Histochem. Cytochem.* 29:1196–1204.
55. Yamada, K. M., and K. Olden. 1978. Fibronectins-adhesive glycoproteins of cell surface and blood. *Nature (Lond.).* 275:179–184.
56. Yamada, K. M., S. Yamada, and I. Pastan. 1976. Cell surface protein partially restores morphology, adhesiveness, and contact inhibition of movement to transformed fibroblasts. *Proc. Natl. Acad. Sci. USA.* 73:1217–1221.